RSC Advances

PAPER

View Article Online
View Journal | View Issue

Cite this: *RSC Adv.*, 2023, **13**, 13128

Facile fabrication of gas sensors based on molybdenum disulfide nanosheets and carbon nanotubes by self-assembly†

Hyejin Rhyu,[ac] Seonjeong Lee,[a] Myunghyun Kang,[b] Daeho Yoon,[c] Sung Myung,*[a] Wooseok Song,[a] Sun Sook Lee[a] and Jongsun Lim[a]

Received 22nd February 2023
Accepted 19th April 2023

DOI: 10.1039/d3ra01183f

rsc.li/rsc-advances

The rising importance of gas detection has prompted rigorous research on flexible and transparent high-performance gas sensors. We demonstrated a sensor for NO_2 detection at room temperature, in which our device was fabricated *via* screen printing on a flexible substrate, and MoS_2 and single-walled carbon nanotube (SWCNT) were coated on a specific area by the self-assembly method. This fabrication process is rapid, facile, and cost-effective. The proposed sensor enables precise and stable NO_2 gas sensing from 50 ppb to 100 ppm. This method should also be applicable to the selective detection of other gases.

1 Introduction

Two-dimensional transition metal dichalcogenides (2D TMDs) have attracted immense research interest in recent years owing to their physical flexibility, unique 2D geometry, and high surface-to-volume ratio.[1–4] In particular, 2D TMDs have shown great promise for use as chemical sensors because of their enhanced sensitivity and room-temperature gas-sensing ability in relation to conventional metal oxides, which generally require high operating temperatures.[5–8] Among the 2D TMDs, MoS_2 has been widely used in thin electronics because MoS_2 nanosheets have unique physical and chemical properties such as optical transparency, flexibility, and tunable band gaps depending on their structure. MoS_2 is a typical 2D TMD used for gas detection owing to its high surface-to-volume ratio, tunable band gap, and high adsorption coefficient.

For application in electrical devices, MoS_2 nanosheets have been synthesized *via* the exfoliation of bulky MoS_2 or chemical vapor deposition through the sulfurization of molybdenum precursors.[9–12] Recently, composites of polymers and 2D semiconducting nanostructures, such as those of MoS_2, have been synthesized to overcome the sensitivity limitations of 2D TMD-based sensors.[13–16] Because 2D carbon-based materials are highly sensitive to gases owing to their intrinsic electrical properties, hybrid layers based on 2D TMDs and graphene with high electron transfer rates and surface-to-volume ratios were utilized to enhance electrochemical and sensing behaviors.[17–19]

One-dimensional carbon nanostructures such as carbon nanotubes (CNTs), graphene oxide (GO), and reduced graphene oxide (rGO) were explored for application as gas sensors. Carbon-based materials have large surface areas for adsorbing gas molecules and high strength and stability.[20–22] In addition, carbon-based materials such as single-walled carbon nanotubes (SWCNTs) were extensively studied as semiconductors for fabricating flexible and sensitive gas sensors, in which SWCNT-based networks are functionalized with polymers, oxide nanoparticles, and other compounds.[23–25]

NO_2, which is emitted by fossil fuel consumption and diesel vehicles, is harmful to both humans and the environment, necessitating its efficient and cost-effective detection.[26–29]

In this study, NO_2 gas sensors were fabricated *via* the selective assembly of nanostructures on the thermoplastic elastomers styrene-ethylene/butylene-styrene (SEBS) and polyurethane (PU), which are stretchable and intrinsically flexible.[30–32] PU has a more hydrophilic surface than SEBS, which causes the MoS_2 nanosheets and SWCNTs to selectively assemble on its surface. Therefore, PU patterns with a hydrophilic surface were utilized to assemble millions of MoS_2/SWCNT nanosheets over large surface areas, while hydrophobic SEBS patterns were used to prevent any unwanted adsorption on nanostructures. Additionally, the MoS_2/SWCNT nanosheets were placed uniformly over the PU surface. A metallic silver electrode was layered on the substrate using screen printing as well. Owing to the wide band gap and flexibility of the MoS_2 nanosheets, the flexibility and gas detection performance of the gas sensors were improved through hybridization of the nanosheets with SWCNTs. The MoS_2/SWCNT-based sensors exhibited NO_2 gas sensitivities of up to 50 ppb at room temperature. As we only used screen printing and selective self-assembly for

[a]*Thin Film Materials Research Center, Korea Research Institute of Chemical Technology (KRICT), 141 Gajeong-ro, Yuseong-gu, Daejeon, 34114, Republic of Korea*
[b]*Advanced Materials Division, Korea Research Institute of Chemical Technology (KRICT), 141 Gajeong-ro, Yuseong-gu, Daejeon 34114, Republic of Korea*
[c]*Department of Advanced Material Science and Engineering, Sungkyunkwan University, Suwon 16419, Republic of Korea*

† Electronic supplementary information (ESI) available. See DOI: https://doi.org/10.1039/d3ra01183f

the fabrication of flexible gas sensors, this approach may lead to the facile industrial-level production of 2D TMD-based devices for practical applications.

2 Experimental

2.1 Synthesis and preparation of MoS_2 nanosheets and SWCNTs

MoS_2 was synthesized using the hydrothermal method. For the synthesis of MoS_2 nanosheets, 1 g of sodium molybdate dihydrate (4.13 mmol) and 1 g of thioacetamide (13 mmol) were dissolved in deionized water (30 mL) and stirred for 30 min. The mixed solution was transferred to a Teflon-lined stainless-steel autoclave, where it underwent hydrothermal reaction at 180 °C for 2 h, after which it was cooled to 25 °C. The resulting suspension was centrifuged with deionized water and ethanol several times to remove the supernatant. The resulting black MoS_2 nanosheets were dried overnight in a vacuum oven at 80 °C. Subsequently, 10 mg of MoS_2 nanosheets, 4 mg of SWCNTs, and 20 mg of sodium dodecylbenzenesulfonate as the suspension agent were suspended in a solution of deionized water (10 mL).

2.2 Fabrication of flexible MoS_2/SWCNT-based gas sensor

SEBS was mixed with toluene in the mass ratio of 2 : 5 and stirred for 24 h at room temperature. The solution was used to fabricate a 120 μm-thick SEBS layer on a polyethylene terephthalate (PET) substrate *via* bar coating using a 4-side applicator. The applicator can be used to adjust the thickness of SEBS. Further, PU was then dissolved in *N*,*N*-dimethylformamide (DMF) in the mass ratio of 1 : 4. PU patterns were fabricated on top of the SEBS layer by screen printing using shadow mask and squeeze in Fig. 1(b) and (c). MoS_2 and SWCNTs were then spin-coated onto the PU and SEBS layers at 2000 rpm for 30 s in Fig. 1(d). Finally, as indicated in Fig. 1(f), the silver electrode was screen-printed on the PU with a channel of 1000 μm and a length of 100 μm shadow mask and squeeze.

2.3 Material characterization and gas-sensing measurements using MoS_2/SWCNT-based gas sensors

The morphologies of the synthesized MoS_2 nanosheets were investigated through transmission electron microscopy (TEM, Titan Cube G2 60-300, FEI company). X-ray diffraction (XRD, Rigaku) was conducted to identify the crystal phase of the synthesized MoS_2 nanosheets with Cu–Kα radiation ($\lambda = 1.5418$ Å) at a current of 40 mA and voltage of 40 kV. For performing chemical-information Raman spectroscopy (inVia Raman spectroscope, Renishaw), X-ray photoelectron spectroscopy (XPS, K-alpha, Thermo Scientific) with an Al–Kα radiation ($h\nu =$ 1486.6 eV) was used to examine the compositions of the MoS_2 nanosheets. The morphological structures of the MoS_2/SWCNT-based gas sensor samples were characterized by field-emission scanning electron microscopy (FE-SEM, Hitachi, S-4700) and energy-dispersive X-ray spectroscopy (EDS).

The electrical properties of the sensors were measured using a semiconductor parameter analyzer (Keithley-4200, Keithley Instruments, USA). NO_2, CO, H_2S, NH_3, acetone, and ethanol gases were individually injected into the sensing chamber to analyze the resistance of the sensors toward them; the sensors were placed 2 cm from the gas inlet, and gas-sensing measurements were carried out at room temperature and under 25% relative humidity.

3 Results and discussion

The screen-printing technique was used to fabricate a MoS_2/SWCNT-based gas sensor, as illustrated in Fig. 1. In the first instance, a 120 μm-thick SEBS layer was fabricated on a PET substrate using the 4-side applicator (Fig. 1(a)). Next, the PU patterns were printed on top of the SEBS layer. When we spin-coated the mixture of MoS_2 and SWCNTs onto the PU and SEBS patterns, we only observed the assembling of nanostructures on the PU pattern, which has a hydrophilic surface. The hydrophobic SEBS layer prevented adsorption on the

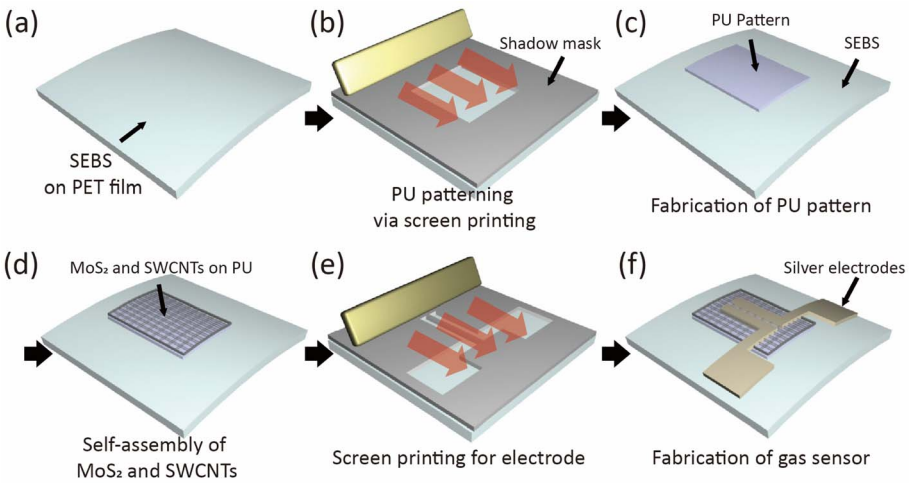

Fig. 1 Schematic of the fabrication process of MoS_2/SWCNT-based gas sensor. (a) Screen printing styrene-ethylene/butylene-styrene (SEBS) on a polyethylene terephthalate (PET) film. (b) Screen printing polyurethane (PU) through shadow mask on SEBS. (c) Fabrication of PU pattern. (d) MoS_2/SWCNT on PU by self-assembly. (e) Screen printing for silver electrode. (f) Fabrication of MoS_2/SWCNT gas sensor.

SWCNTs. Then, Fig. 2(a)–(d) displays the results of the TEM, XRD, Raman spectroscopy and XPS analyses for the synthesized MoS_2. As shown in Fig. 2(a(i)) the interlayer distance of the MoS_2 nanosheets was approximately 0.65 nm, which corresponds to the (002) plane of bulk MoS_2. The lattice *d*-spacing was estimated to be 0.25 nm, which corresponds to the (100) lattice plane of the MoS_2 phase; this concurs with the XRD results. Fig. 2(a(ii)) MoS_2 selected area electron diffraction (SAED) patterns indicating the hexagonal lattice structure of MoS_2 nanosheets. Fig. 2(a(iii) and (iv)) displays crumpled MoS_2 nanosheets with a size of hundreds of nanometers.

Fig. 2(b) illustrates the XRD spectra of the MoS_2 nanosheets; the characteristic peaks of the MoS_2 nanosheets were observed at 11.52°, 33.90°, and 56.62°, corresponding to the (002), (100), and (110) planes, respectively. Fig. 2(c) represents the Raman spectra (λ_{exc} = 532 nm) displaying the signals for the in-plane vibrational mode (E^1_{2g}) and out-of-plane vibrational mode (A_{1g}) of MoS_2 at 383.02 and 408.14 cm^{-1}, respectively. Fig. 2(d) illustrates the XPS results for Mo 3d and S 2p. For Mo 3d, two strong peaks are located at 229.6 and 232.8 eV, which can be ascribed to Mo $3d_{5/2}$ and Mo $3d_{3/2}$. The small peak at 226.8 eV was assigned to the S 2s of MoS_2. Other observed peaks at 162.4 and 163.6 eV were assigned to S in 2H–MoS_2. This confirms the successful synthesis of MoS_2.

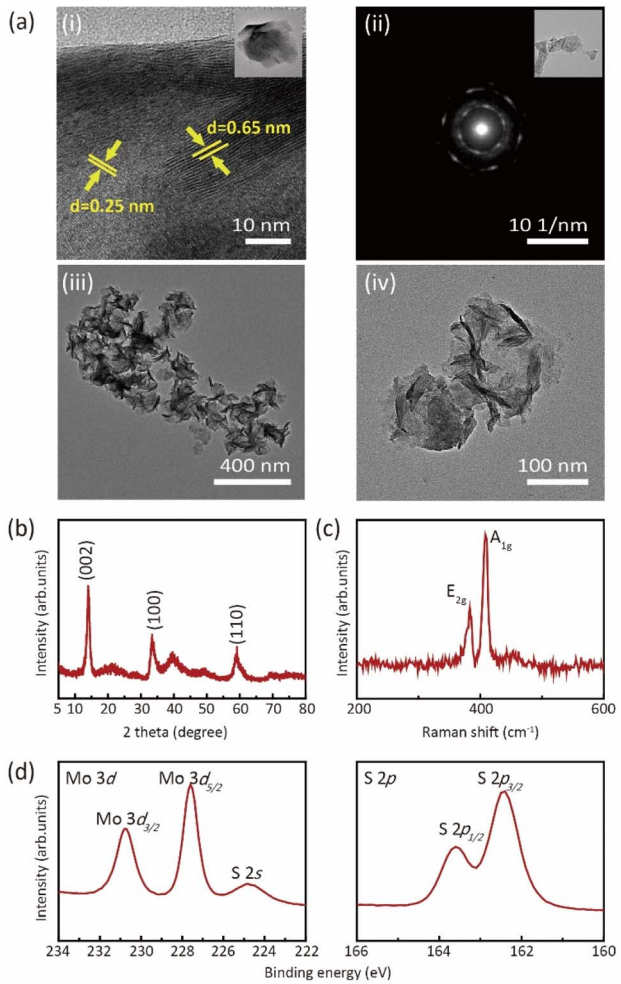

Fig. 2 (a) Transmission electron microscopy (TEM) images of MoS_2 nanosheets: (i) TEM images of MoS_2 show the lattice distance. (ii) Selected area electron diffraction (SAED) pattern. (iii and iv) TEM images of MoS_2 nanosheets. (b) X-ray diffraction (XRD) patterns of MoS_2 nanosheets (c) Raman spectra of MoS_2. X-ray photoelectron spectroscopy (XPS) spectra of (d) Mo 3d and S 2p.

Fig. 3(a) depicts the SEM images of PU and SEBS after the assembly of MoS_2 and the SWCNTs. These results indicate that, upon spin coating, both MoS_2 nanosheets and SWCNTs assembled selectively on the PU region, and SWCNTs could not be observed on the hydrophobic SEBS surface. Here, the density of MoS_2/SWCNT adhering to the PU surface can be controlled by adjusting the concentration of the MoS_2/SWCNT solution. The hydrophilic surface of PU adsorbed MoS_2 and SWCNTs, and the hydrophobic SEBS layer repelled SWCNTs. The EDS measurements also confirmed the uniform assembly of MoS_2/SWCNT network patterns on the PU substrate (Fig. 3(b)). The MoS_2/SWCNT network on PU was composed of O, S, Mo, and C. Finally, a silver layer with a channel of 1000 μm and length of 100 μm was screen-printed on the PU surface. It acts as the conductive metallic layer required to complete the fabrication of the MoS_2/SWCNT-based gas sensors. As indicated in the SEM images and EDS analyses of PU and SEBS boundary after the assembly of MoS_2 and the SWCNTs, MoS_2 nanosheets were assembled on both PU and SEBS, whereas the SWCNTs were observed only on PU (Fig. S1 in ESI†). Additionally, the MoS_2/SWCNT assembled on PU was analyzed by using XPS in order to confirm the chemical state and bonding of MoS_2/SWCNT in Fig. S2 in ESI.†

Fig. 4(a) shows the response of the sensor to 100 ppm NO_2 observed during the two testing cycles at room temperature; the cyclic nature of the response demonstrates the sensor's repeatable gas response and recovery in Fig. S3 in ESI.† It is well-known that, in the presence of MoS_2 and SWCNTs, NO_2 acts as an electron acceptor while NH_3 acts as an electron donor. These results clearly demonstrated the enhanced response of the MoS_2/SWCNT system to both NO_2 and NH_3, in which the resistance of the device decreased with NO_2 adsorption and increased with NH_3 adsorption. In previous reports, p-type carbon materials, such as graphene or SWCNTs functionalized with n-type MoS_2 nanosheets were found to behave as p-type materials. Similarly, the analyses led us to conclude that the proposed MoS_2/SWCNT hybrid structure was a p-type semiconductor material. The sensing mechanism of the NO_2 gas-sensor MoS_2/SWCNT was explained as in previous references. As NO_2 gathers a free electron from the MoS_2 and SWCNTs, MoS_2/SWCNT exhibits p-type semiconductor properties. The two components cause the generation of more holes when hybridized. Hence, when the sensor was exposed to NO_2, its resistance decreased and sensitivity increased. We performed a cycling test to evaluate the stability of the gas sensors in Fig. 4(a). The curves exhibited reproducible responses when air and NO_2 were injected alternately. The sensor exhibited a sensitivity of 88% to 100 ppm of NO_2 at room temperature. The gas sensitivity was calculated as $\Delta R/R_a = (R_g - R_a)/R_a$, where R_a and R_g are the resistances of the sensor to synthetic air and the target gas, respectively.[14,33–35]

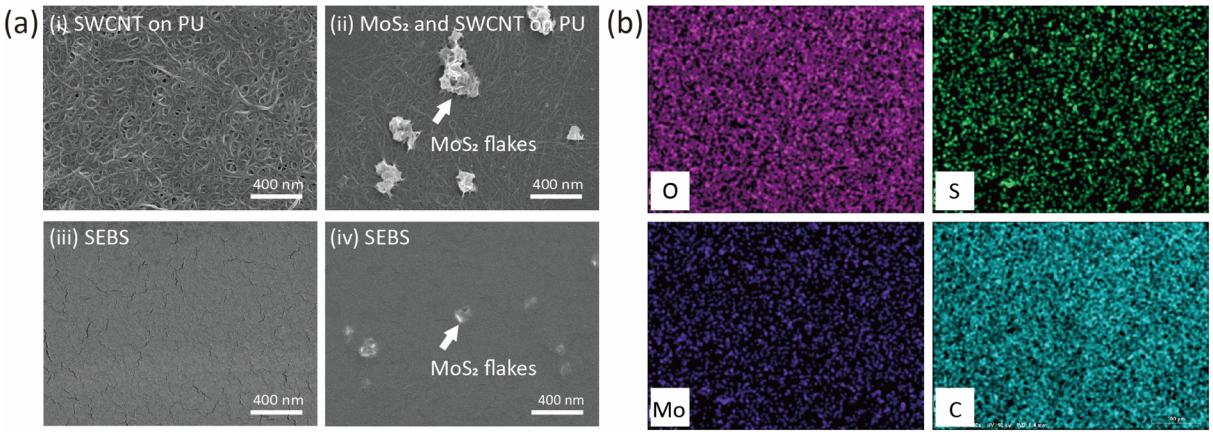

Fig. 3 (a) Scanning electron microscopy (SEM) images of MoS_2/SWCNT on PU and SEBS: (i) SWCNTs self-assembly on PU (ii) MoS_2/SWCNT self-assembly on PU (iii) SWCNTs on SEBS (iv) MoS_2/SWCNT on SEBS (b) energy dispersive spectroscopy (EDS) elemental mapping of MoS_2/SWCNT O, S, Mo, and C elements on PU substrate.

At various NO_2 concentrations, the detection limit for NO_2 gas ranged from 50 ppb to 1 ppm (Fig. 4(b)). In Fig. 4(b), detection of 50 ppb of NO_2 can be regarded as the minimum detection limit of the MoS_2/SWCNT gas sensor, with a response value of 4.5%. These results indicate good performance compared to other studies for NO_2 gas sensors using MoS_2 and graphene hybrid materials in Table S1 in ESI.† When the concentration was increased from 50 ppb to 1 ppm, the response increased proportionally (Fig. 4(c)). As the relationship between concentration and sensitivity was linear, we concluded that the structure of the nanomaterial did not affect the sensing performance; therefore, the proposed fabrication method can be used with any nanoscale material, including nanowires, nanotubes, and nanoparticles. The response of the MoS_2/SWCNT-based gas sensor to various other gases (CO, H_2S, NH_3, acetone vapor, and ethanol vapor) at room temperature was also investigated (Fig. 5). We tested 100 ppm of a specific gas at room temperature in two cycles. The responses to CO, H_2S, and NH_3 were 2.6%, 7.8%, and 14.8%, respectively, with no response to acetone or ethanol gases in Fig. 5(a)–(e). In contrast to the resistance change caused by NO_2, the resistance of the MoS_2/SWCNT-based gas sensor to NH_3 and H_2S gases increased with the adsorption of their molecules. This is because NO_2 accepts electrons, whereas NH_3 and H_2S act as electron donors. The response value of 100 ppm NO_2 was 11.3 times that of 100 ppm H_2S and 5.9 times that of 100 ppm NH_3 (Fig. 5(f)). This substantiates the gas sensor's excellent selectivity to NO_2 at room temperature.

As illustrated in Fig. 4, the response of the sensor decreases for NO_2 gas. First, the material is exposed to air, and O_2 molecules are adsorbed and form O_2^- ions on the material surface.

$$O_2\,(g) + e^- \rightarrow O_2^-\,(ads)$$

Upon exposure to the material, NO_2 gas becomes NO_2^- by accepting electrons from the O_2^- ions.

$$NO_2\,(g) + e^- \rightarrow NO_2^-\,(ads)$$

$$NO_2\,(g) + O_2^-\,(ads) + 2e^- \rightarrow NO_2^-\,(ads) + 2O^-$$

This confirms that the gas-sensing material increased the concentration of holes on the surface of the material. As shown

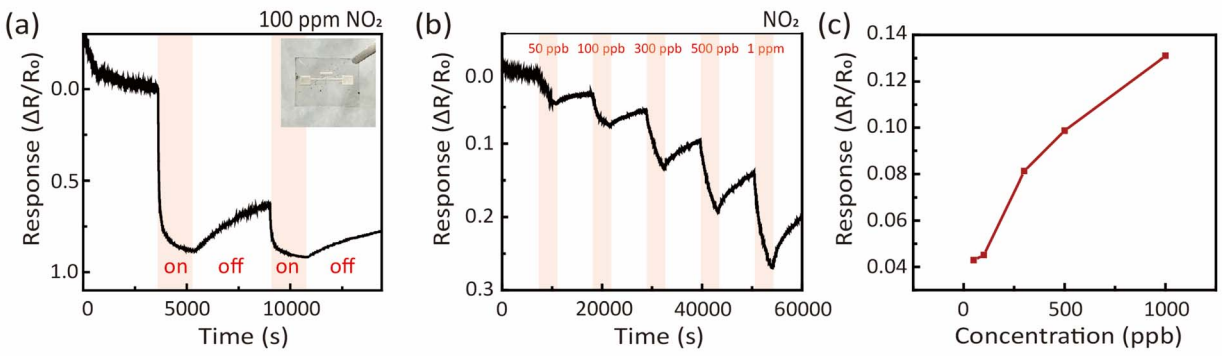

Fig. 4 The response of NO_2 gas at room temperature. (a) Two successive sensing responses at NO_2 100 ppm, (b) dynamic responses and recovery curves of MoS_2/SWCNT gas sensor towards NO_2 gas at room temperature (c) fitting curve of response *versus* concentration.

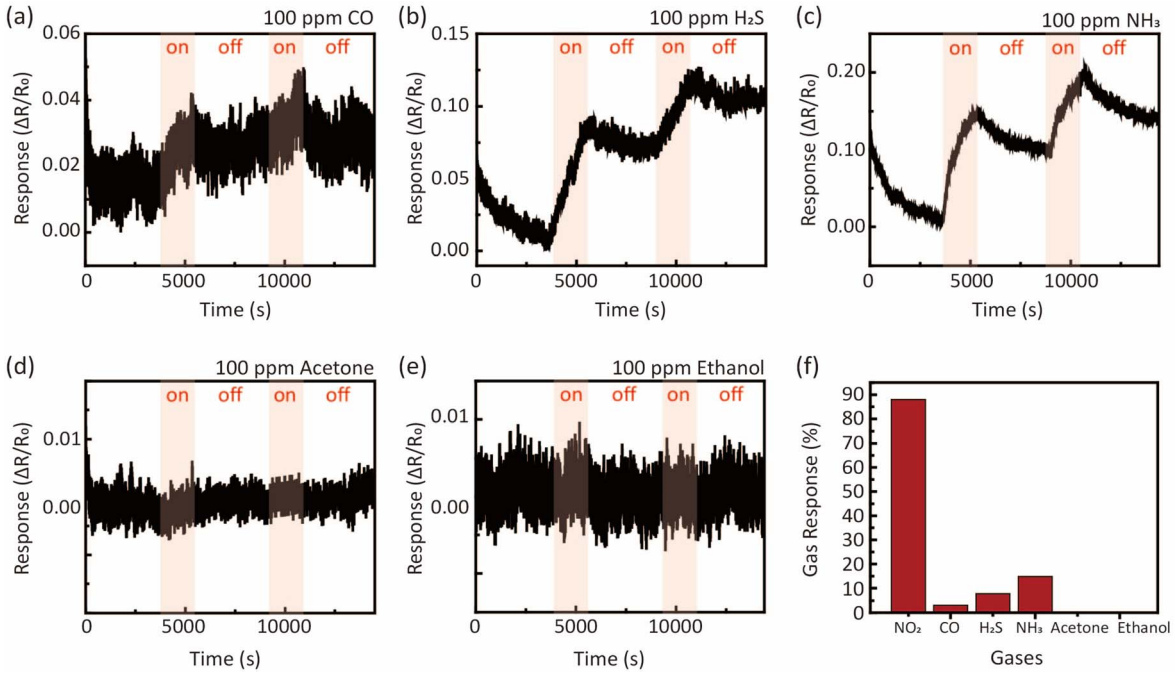

Fig. 5 Gas response performance of MoS_2/SWCNT sensor at room temperature 100 ppm. (a) CO gas response, (b) H_2S gas response, (c) NH_3 gas response, (d) acetone gas response, (e) ethanol gas response, and (f) gas selectivity summary of the sensor to various gases at room temperature.

in Fig. 5(c), the transient resistance responses of the sensor to NO_2 and NH_3 were compared. In contrast to the resistance change caused by NO_2, the resistance increased when exposed to NH_3 because the MoS_2/SWCNT sensor is a p-type semiconductor.

$$O_2\ (g) + e^- \rightarrow O_2^-\ (ads)$$

$$2NH_3\ (ads) + 3O_2^- \rightarrow N_2\ (g) + 3H_2O + 3e^-$$

$$NH_3\ (ads) + OH^- \rightarrow NH_2 + H_2O + e^-$$

When the MoS_2/SWCNT-based sensor was exposed to NH_3, following this mechanism, the O species reacted with NH_3. Then the electrons were released back to MoS_2/SWCNT, causing an increase in the electron concentration in the conduction band of MoS_2. The transferred electrons recombined with the carriers, thus decreasing the charge carrier concentration and consequently increasing the electrical resistance.[34–36] Therefore, owing to the synergistic actions of MoS_2 and SWCNTs, the MoS_2/SWCNT-based gas sensor exhibited high sensitivity to NO_2 gas.

4 Conclusions

We demonstrated a facile method of fabricating high-performance MoS_2/SWCNT-based gas sensors *via* screen printing, making it a rapid, simple, and cost-effective technology. While MoS_2 assembled itself on both SEBS and PU, the SWCNTs attached only to the hydrophilic PU; therefore, MoS_2/SWCNT hybrid nanostructures were successfully assembled on PU substrates. The MoS_2/SWCNT-based gas sensor exhibited high selectivity for NO_2 at room temperature, as well as high performance, reliable response, and recovery. In particular, the response to 100 ppm NO_2 at room temperature was 11.3 and 5.9 times higher than that to 100 ppm H_2S and NH_3, respectively. Moreover, the hybrid gas sensor was fabricated on a flexible substrate; therefore, it should be applicable in sensitive wearable electronics.

Conflicts of interest

There are no conflicts to declare.

Acknowledgements

This research was supported by the Nanomaterial Technology Development Program through the National Research Foundation of Korea (NRF) funded by the Ministry of Science and ICT (NRF-2021M3H4A3A02086431).

Notes and references

1 M. Chhowalla, H. S. Shin, G. Eda, L.-J. Li, K. P. Loh and H. Zhang, *Nat. Chem.*, 2013, **5**, 263–275.
2 K. F. Mak and J. Shan, *Nat. Photon.*, 2016, **10**, 216–226.
3 J. W. Seo, Y. W. Jun, S. W. Park, H. Nah, T. Moon, B. Park, J. G. Kim, Y. J. Kim and J. Cheon, *Angew. Chem., Int. Ed.*, 2007, **46**, 8828–8831.
4 M. Chhowalla, Z. Liu and H. Zhang, *Chem. Soc. Rev.*, 2015, **44**, 2584–2586.

5 K. Lee, R. Gatensby, N. McEvoy, T. Hallam and G. S. Duesberg, *Adv. Mater.*, 2013, **25**, 6699–6702.
6 K. Y. Ko, J.-G. Song, Y. Kim, T. Choi, S. Shin, C. W. Lee, K. Lee, J. Koo, H. Lee and J. Kim, *ACS Nano*, 2016, **10**, 9287–9296.
7 X. Liu, T. Ma, N. Pinna and J. Zhang, *Adv. Funct. Mater.*, 2017, **27**, 1702168.
8 S. Hussain, A. J. Khan, M. Arshad, M. S. Javed, A. Ahmad, S. S. A. Shah, M. R. Khan, S. Akram, S. Ali and Z. A. ALOthman, *Ceram. Int.*, 2021, **47**, 8659–8667.
9 F. K. Perkins, A. L. Friedman, E. Cobas, P. M. Campbell, G. G. Jernigan and B. T. Jonker, *Nano Lett.*, 2013, **13**, 668–673.
10 L.-C. Wang, S.-K. Bao, J. Luo, Y.-H. Wang, Y.-C. Nie and J.-P. Zou, *Int. J. Hydrogen Energy*, 2016, **41**, 10737–10743.
11 B. Liu, L. Chen, G. Liu, A. N. Abbas, M. Fathi and C. Zhou, *ACS Nano*, 2014, **8**, 5304–5314.
12 J. Park, J. Mun, J.-S. Shin and S.-W. Kang, *R. Soc. Open Sci.*, 2018, **5**, 181462.
13 Y. Zhao, J.-G. Song, G. H. Ryu, K. Y. Ko, W. J. Woo, Y. Kim, D. Kim, J. H. Lim, S. Lee, Z. Lee, J. Park and H. Kim, *Nanoscale*, 2018, **10**, 9338–9345.
14 G. Deokar, P. Vancso, R. Arenal, F. Ravaux, J. Casanova-Cháfer, E. Llobet, A. Makarova, D. Vyalikh, C. Struzzi and P. Lambin, *Adv. Mater. Interfaces*, 2017, **4**, 1700801.
15 Z. S. Mahmoudabadi, A. Tavasoli, A. Rashidi and M. Esrafili, *Environ. Sci. Pollut. Res. Int.*, 2021, **28**, 5978–5990.
16 X.-H. Tian, T.-Y. Zhou, Y. Meng, Y.-M. Zhao, C. Shi, P.-X. Hou, L.-L. Zhang, C. Liu and H.-M. Cheng, *Molecules*, 2022, **27**, 6523.
17 S. Hussain, N. Farooq, A. S. Alkorbi, R. Alsaiari, N. A. Alhemiary, M. Wang and G. Qiao, *J. Mol. Liq.*, 2022, **362**, 119765.
18 S. Hussain, X. Yang, M. K. Aslam, A. Shaheen, M. S. Javed, N. Aslam, B. Aslam, G. Liu and G. Qiao, *Chem. Eng. J.*, 2020, **391**, 123595.
19 N. Farooq, S. Hussain, A. S. Alkorbi, A. M. Qureshi, M. A. Wattoo, R. Alsaiari, N. A. Alhemiary and A. ur Rehman, *Surf. Interfaces*, 2022, **32**, 102116.
20 S. Hussain, M. S. Javed, S. Asim, A. Shaheen, A. J. Khan, Y. Abbas, N. Ullah, A. Iqbal, M. Wang and G. Qiao, *Ceram. Int.*, 2020, **46**, 6406–6412.
21 P. Dariyal, S. Sharma, G. S. Chauhan, B. P. Singh and S. R. Dhakate, *Nanoscale Adv.*, 2021, **3**, 6514–6544.
22 N. Iqbal, A. Afzal, N. Cioffi, L. Sabbatini and L. Torsi, *Sens. Actuators, B*, 2013, **181**, 9–21.
23 P. B. Agarwal, B. Alam, D. S. Sharma, S. Sharma, S. Mandal and A. Agarwal, *Flexible Printed Electron.*, 2018, **3**, 035001.
24 S. Tang, W. Chen, H. Zhang, Z. Song, Y. Li and Y. Wang, *Front. Chem.*, 2020, **8**, 174.
25 I. Dube, D. Jiménez, G. Fedorov, A. Boyd, I. Gayduchenko, M. Paranjape and P. Barbara, *Carbon*, 2015, **87**, 330–337.
26 M. W. Frampton, J. Boscia, N. J. Roberts Jr, M. Azadniv, A. Torres, C. Cox, P. E. Morrow, J. Nichols, D. Chalupa and L. M. Frasier, *Am. J. Physiol.: Lung Cell. Mol.*, 2002, **282**, 155–165.
27 S. Basu and P. Bhattacharyya, *Sens. Actuators, B*, 2012, **173**, 1–21.
28 W. Yang, L. Gan, H. Li and T. Zhai, *Inorg. Chem. Front.*, 2016, **3**, 433–451.
29 S. Hussain, N. Ullah, Y. Zhang, A. Shaheen, M. S. Javed, L. Lin, S. B. Shah, G. Liu and G. Qiao, *Int. J. Hydrogen Energy*, 2019, **44**, 24525–24533.
30 G.-J. Zhu, P.-G. Ren, H. Guo, Y.-L. Jin, D.-X. Yan and Z.-M. Li, *ACS Appl. Mater. Interfaces*, 2019, **11**, 23649–23658.
31 J. Cao and X. Zhang, *J. Appl. Phys.*, 2020, **128**, 220901.
32 J. Zeng, W. Ma, Q. Wang, S. Yu, M. T. Innocent, H. Xiang and M. Zhu, *Compos. Commun.*, 2021, **25**, 100735.
33 F. Schedin, A. K. Geim, S. V. Morozov, E. W. Hill, P. Blake, M. I. Katsnelson and K. S. Novoselov, *Nat. Mater.*, 2007, **6**, 652–655.
34 B. Cho, J. Yoon, S. K. Lim, A. R. Kim, D.-H. Kim, S.-G. Park, J.-D. Kwon, Y.-J. Lee, K.-H. Lee and B. H. Lee, *ACS Appl. Mater. Interfaces*, 2015, **7**, 16775–16780.
35 H. S. Hong, N. H. Phuong, N. T. Huong, N. H. Nam and N. T. Hue, *Appl. Surf. Sci.*, 2019, **492**, 449–454.
36 N. Donato, M. Latino and G. Neri, *Carbon Nanotubes: Res. Appl.*, 2011, **14**, 229–242.